Spectral and statistical properties of strongly driven atoms coupled to frequency-dependent photon reservoirs

M. Lewenstein*
Department of Physics, Harvard University, Cambridge, Massachusetts 02138

T. W. Mossberg
Department of Physics, University of Oregon, Eugene, Oregon 97403

(Received 8 September 1987)

Interesting new aspects of atomic behavior in the presence of strong driving fields appear when the driven atom resides not in free space, but in a region (such as an optical cavity) that displays a frequency-dependent photon-mode density. Under such conditions, it is found that a strong driving field can modify the spontaneous decay properties of an atom, and thereby give rise to interesting new features in the spectrum of strong-field resonance fluorescence. It is also found that a high level of dressed-state polarization can be maintained in a sample of resonantly or nonresonantly driven atoms by appropriate tuning of an enclosing cavity. Furthermore, for appropriate laser and cavity tunings, it is found that the atomic states become highly squeezed. In the course of analyzing these effects, a set of modified Bloch equations is derived that explicitly accounts for the finite response time associated with a frequency-dependent photon-mode density.

I. INTRODUCTION

In this paper we analyze the spectral and statistical properties of atoms driven by a strong, single-mode, light field and coupled to a reservoir of electromagnetic field modes whose spectral density displays a strong frequency dependence. One realization of this system consists of a driven atom confined within an optical cavity. As a preliminary, we discuss recent work in the area of cavity quantum electrodynamics, and attempt to place the present results in proper context with it.

In 1946, Purcell[1] predicted that the spontaneous-emission rate of an atom located in a cavity tuned to the atomic-transition frequency would be substantially larger than in free space. The enhancement results from a cavity-induced increase in photon-mode density at the atomic-transition frequency. Following this idea, Kleppner[2] predicted that the opposite effect, i.e., suppression of spontaneous emission, occurs if a cavity is employed to reduce the density of photon modes in the spectral region of the atomic transition. In fact, Kleppner predicted that spontaneous-emission could be eliminated altogether by placing an atom in a wave guide below cutoff. Kleppner's paper stimulated a series of experimental works on this subject[3] in both the microwave and optical regimes. In most of the experiments, the dimension of the cavity was comparable to the wavelength. Quite recently, however, Heinzen *et al.*[4] showed that analogous effects can be observed in confocal cavities of large dimensions.

We have recently shown that modifications of spontaneous-emission rates may be effected not only with the essentially passive means described above, but also through a dynamical means,[5] i.e., by imposing a strong driving field on the atoms. In order for such a dynamical effect to occur, the atoms must reside in a region of space in which the density of photon modes varies appreciably on a frequency scale set by the Rabi frequency of the driving field. Cavities provide a natural setting for finding such frequency-dependent mode densities, but they may also arise in diverse environments, including those involving the solid state. One purpose of this paper is to present a detailed treatment of the effect of strong driving fields on spontaneous-emission rates in the particular situation where the irradiated atom is within a cavity. We analyze resonance-fluorescence spectra for features indicative of dynamical modifications of spontaneous emission. As we will see below, the spectra also reveal other novel effects such as the polarization of the atom-field dressed-state populations.

A second area of cavity quantum electrodynamics of recent interest deals with the spectral and statistical aspects of collective[6] and single-atom behavior. Studies[7] involving the role of quantum fluctuations in optical bistability have led to the prediction of small photon antibunching[8] and squeezing[9] effects. These effects are, in fact, related to the photon antibunching and squeezing found in the study of resonance fluorescence of a single two-level atom in free space.[8,10] This relation has been established by Carmichael[11] and extended to multi-atom systems by Lugiato.[12] New insight into the statistical properties of the quantum electromagnetic field in cavities has been achieved with the discovery of the vacuum Rabi splitting,[13] which can be alternatively considered as another type of modification of the spontaneous-emission process. In the regime, when the cavity width Γ becomes comparable or smaller than the atomic spontaneous-emission rate, the resonance-fluorescence spectrum consists of two separate peaks. The splitting reflects the splitting of the lowest excited energy levels in the Jaynes-Cummings[14] model. Recently, Raizen *et al.*[15] studied the light transmitted through an atom-containing cavity and observed substantial relative squeezing.

We have investigated a number of quantum-statistical aspects of strongly driven atoms in cavities, i.e., strongly driven atoms coupled to frequency-dependent photon-mode reservoirs. Under the conditions of strong or moderate driving-field strengths and nonvanishing detunings between the atomic, laser, and cavity frequencies, large atomic-squeezing effects have been found.[16] The atomic squeezing exhibits itself as a squeezing of the scattered-light field. Although the squeezing of the scattered light is not as large in relative terms as the squeezing of the atoms, the optical squeezing arises in a regime quite unexpected on the basis of free-space results.[10] The present paper contains a detailed analysis of these effects.

While not of direct relevance to the present paper, we note that the study of Rydberg atoms in ultrahigh Q cavities[17] has recently received a great deal of attention. In this regime, a Jaynes-Cummings[14] model provides a good starting point for the theory. Numerous novel effects have been discussed and observed in this framework, such as atomic collapse[18] and revivals,[19,20] single-atom masers,[21] etc.

The remaining sections of the present paper are organized as follows. Section II provides a simple qualitative explanation of dynamical modifications of spontaneous emission and related effects. In Sec. III we describe in detail our model and discuss the method we use to solve the appropriate equations of motion. The main result here is to obtain modified Bloch equations describing the evolution of the mean atomic inversion and polarization in a region of space, e.g., a cavity, exhibiting a strongly frequency-dependent spectral density of photon modes. These equations are obtained for arbitrary mode-density functions, provided that the mode density is essentially constant over the radiative width of the atom, and for driving-field Rabi frequencies larger than atomic radiative width. Section IV is devoted to the discussion of fluorescence power spectra. We present there the method of calculating the spectra and present closed-form approximate formulas for heights, widths, and positions of the peaks in a modified Mollow[22] spectrum. We also present there some new numerical results, concerning the case of nonvanishing detunings as well as non-Lorentzian mode-density functions. In Sec. V we discuss quantum-statistical properties, such as squeezing, of strongly driven atoms in the presence of a frequency-dependent photon-mode density. Finally, in the Appendix, we present the full set of equations for single-time, atom-field correlations which can be used for a systematic extension of our results into broader parameter regions than allowed for under the approximations employed in the present paper. Throughout, we assume that optical or microwave cavities provide a convenient means of achieving the frequency-dependent photon-mode density central to our analysis.

II. DYNAMICAL MODIFICATIONS OF SPONTANEOUS EMISSION

The effects of interest here are all of a fundamentally quantum nature. Nevertheless, considerable intuitive insight and understanding can be gained by the discussion of these effects within the framework of the semiclassical Bloch picture. The Bloch equations in the absence of detuning, damping, and in the rotating frame have the form[23]

$$\frac{d\boldsymbol{\sigma}}{dt}=\boldsymbol{\Omega}\times\boldsymbol{\sigma}\ , \tag{1}$$

where $\boldsymbol{\sigma}=(\sigma_1,\sigma_2,\sigma_3)$ is the Bloch vector and $\boldsymbol{\Omega}$, whose magnitude is equal to the Rabi frequency Ω, is the pseudofield vector. For convenience, $\boldsymbol{\Omega}$ is assumed throughout to point along the x direction, i.e., $\boldsymbol{\Omega}=(\Omega,0,0)$. The solutions of Eq. (1) describe the precession of a spin vector $\boldsymbol{\sigma}$ around the $\boldsymbol{\Omega}$ axis. In particular, the σ_1 component of the Bloch vector, which is parallel to the driving field $\boldsymbol{\Omega}$ (or, in other words, which is in phase with the driving field) remains constant. If we prepare the system in a state such that $\boldsymbol{\sigma}$ is initially parallel to $\boldsymbol{\Omega}$, the Bloch vector will, in the absence of damping, stay in this position forever. This phenomenon is sometimes referred to as spin locking.[24] We now consider the effect of damping.

In the case of an isolated two-level atom, the most important damping mechanism is spontaneous radiative decay, and this mechanism is associated with the coupling of the atom to the zero-point electromagnetic fields. We may, therefore, try to model the effects of these fluctuations, within the framework of the semiclassical picture, by introducing a driving field with small classical fluctuations,

$$\boldsymbol{\Omega}(t)=\boldsymbol{\Omega}+\delta\boldsymbol{\Omega}(t)\ . \tag{2}$$

These fluctuations are expected to trigger the decay of the Bloch vector from the semiclassical trajectory to its stationary state. One can easily perform a linear stability analysis of the Bloch vector precession with respect to field fluctuations $\delta\boldsymbol{\Omega}(t)$, and one makes two basic observations.

(a) Fluctuations induce a change of the in-phase component of the polarization σ_1, which is proportional to the time average of $\delta\Omega_3(t)\sigma_2(t)-\delta\Omega_2(t)\sigma_3(t)$. Since σ_2 and σ_3 (in the lowest order) undergo Rabi oscillations, the fluctuation-induced variation of σ_1 is significant if and only if the field fluctuation $\delta\boldsymbol{\Omega}(t)$ contains Fourier components at the frequencies $\pm\Omega$ (or $\omega_0\pm\Omega$ in the nonrotating frame, where ω_0 is the atomic transition frequency). In particular, if $\delta\boldsymbol{\Omega}(t)$ only contains spectral components whose frequencies are much smaller than Ω, the σ_1 component will adiabatically follow the motion of $\boldsymbol{\Omega}(t)$ and remain largely constant.

(b) The σ_2 and σ_3 components of the Bloch vector are sensitive not only to Fourier components of $\delta\boldsymbol{\Omega}$ at the frequencies $\pm\Omega$ but also to those at zero frequency. This means that fluctuation-induced variations of σ_2 and σ_3 will be non-negligible even if $\delta\boldsymbol{\Omega}(t)$ only contains frequencies close to zero.

On the basis of these observations, one can conclude that the Rabi frequency provides a means of controlling which reservoir spectral components contribute to Bloch-vector damping. If the reservoir exhibits *spectral structure*, it follows that variations in *Rabi frequency* may lead to changes in the *Bloch-vector damping rate.* In free space both in the optical and microwave regime, the spectrum of the vacuum fluctuations, or, alternatively, the density of photon modes, is practically constant, and one would not expect a dynamical modification of spontaneous decay rates. The situation may be dramatically different in appropriately designed cavities. There, as we mentioned, the photon-mode density may be strongly frequency dependent, and exhibit maxima and minima. In passive experiments, the frequency dependence of the cavity photon-mode density leads to enhancement or inhibition of spontaneous-emission rates above or below their free-space values.

Consider then a driven atom in a cavity. We assume that the atomic frequency ω_0, laser frequency ω_l, and cavity frequency ω_c are all equal. Suppose that we prepare[25,26] an atom in one of the dressed states (so that initially the Bloch vector is parallel to $\mathbf{\Omega}$). If the Rabi frequency Ω is much smaller than the cavity width Γ (so that the frequencies $\pm\Omega$ lie close to the maximum in the photon-mode density), the Bloch vector will be driven away from the locked position and tend toward the stationary state. On the other hand, if the Rabi frequency Ω is much larger than the cavity width (so that the frequencies $\pm\Omega$ lie in a spectral region of low-photon-mode density), there will be practically no vacuum fluctuations in the cavity to trigger the decay. The σ_1 component of the Bloch vector (which corresponds to the population inversion of the dressed states[25,26]) will remain constant for a very long time.

Note that the two other components of the Bloch vector will, in fact, attain their stationary values relatively rapidly even for $\Omega \gg \Gamma$. This is due to the fact that their decay may be triggered by vacuum fluctuations at zero frequency (corresponding to modes at the center of the cavity resonance where the mode density is high) as well as by fluctuations at frequencies $\pm\Omega$. We should, however, expect that for $\Omega \gg \Gamma$, the damping of σ_2 and σ_3 (which correspond to the dressed-state coherence) may be reduced.

All the effects discussed above should be reflected in the power spectrum of resonance fluorescence. For $\Omega \ll \Gamma$ we should not expect any departures from the standard Mollow[22] result (expect that the high mode density in the cavity will lead to a broadening of the Mollow peaks). However, for $\Omega \gg \Gamma$, we should expect a dramatic narrowing of the central peak, which corresponds to a suppression of the decay rate of σ_1. Since the decay rates of σ_2 and σ_3 can be reduced only a limited amount, the narrowing of the sideband peaks should be less pronounced. Of course the intuitive ideas presented above must be carefully and quantitatively analyzed on the level of modified Bloch equations. Independently, they should be analyzed on the level of equations for two-time, atomic correlation functions since the quantum regression theorem does not hold.[27] As we have show in abbreviated form[5] such analysis does indeed confirm the intuitive conclusions outlined above.

An intuitive analysis may also be presented in the case of nonvanishing laser-atom detuning $\Delta_1 \equiv \omega_l - \omega_0$ and/or laser-cavity detuning $\Delta_2 \equiv \omega_l - \omega_c$. In such cases, the semiclassical Bloch motion is sensitive to fluctuations of the characteristic frequencies $0, \pm(\Omega^2+\Delta_1^2)^{1/2}$. Since the cavity supports only the vacuum fluctuations of the characteristic frequency Δ_2 (viewed as usual from the frame rotating at the laser frequency), we may again by appropriate choice of parameters modify (i.e., enhance or suppress) the damping rates of the dressed-state inversion and coherence. The detailed discussion of these effects and their relation to squeezing accompanies the presentation of the numerical results in Sec. IV of this paper and in Ref. 16.

It should be stressed that the driving-field-induced modification of radiative damping predicted here follows from the same essential physics that gives rise to the field-dependent damping analyzed in other contexts. These other contexts include solid- and gas-phase relaxation,[28] atoms exposed to strong incoherent fields,[29] laser phase fluctuations and their effect,[30,31] and autoionization spectra.[32,33] As mentioned previously, dynamical narrowing or broadening of spectral lines, can be expected in any case where one considers the interaction of an atom with a reservoir that exhibits a suitably structured spectrum. In the present example, the only requirement on the spectral structure turns out to be one of scale (relative to the Rabi frequency). The situation may be more complicated in other physical systems.[30–32] In a cavity, the reservoir spectral structure is simple, consisting of periodic peaks superimposed on a more or less constant background. The background arises from the open sides of the optical cavity.

III. THE MODEL

An experiment in which the effect discussed above should be observable consists of the following: An atomic beam is injected into an optical cavity and is driven by a laser beam. The laser light may be injected directly into the cavity modes (which eventually flows away from the cavity through the mirrors) or into the side modes. Field-dependent effects are to be monitored through their effect on the atomic-fluorescence spectrum.

The Hamiltonian for this system may be written ($c=\hbar=1$)

$$\mathcal{H}=\mathcal{H}_A+\mathcal{H}_{AF}+\mathcal{H}_F , \tag{3}$$

where the free atomic Hamiltonian is

$$\mathcal{H}_A=\left[\frac{\omega_0}{2}\right]\hat{\sigma}_3 , \tag{4}$$

ω_0 is the atomic-transition frequency, and $\hat{\sigma}_3$ the atomic inversion operator. The free-field Hamiltonian consists of two parts

$$\mathcal{H}_F=\int dk\, \hat{c}_k^{\dagger}\hat{c}_k+\int dk\, \hat{b}_k^{\dagger}\hat{b}_k . \tag{5}$$

In Eq. (5) the reservoir has been divided into two parts, one consisting of so-called cavity modes ($\hat{c}$) and the other background modes ($\hat{b}$). The density of cavity modes is large only in the vicinity of the cavity resonance frequency ω_c. Geometrically, their spatial structure is close to that of the cavity resonant mode. On the other hand, background modes contribute equally at all the frequencies. Their density sets a lower limit for spontaneous decay rates of atoms whose transition frequencies are far from ω_c. Their spatial structure is quite different from the cavity resonant mode. In the process of fluorescing into the cavity mode, the cavity photons (described by $\hat{c}_k^\dagger,\hat{c}_k$) are created. Fluorescence out the side of the cavity creates background photons.

The atom-field interaction Hamiltonian consists of three terms,

$$\mathcal{H}_{\rm AF}=\frac{\Omega}{2}(\hat{\sigma}e^{i\omega_l t}+\hat{\sigma}^\dagger e^{-i\omega_l t})+\int[g_c(k)\hat{\sigma}^\dagger\hat{c}_k+\text{H.c.}]dk + \int[g_b(k)\hat{\sigma}^\dagger\hat{b}_k+\text{H.c.}]dk \ . \quad (6)$$

The first term describes the interaction with the coherent, monochromatic laser wave of frequency ω_l. The strength of this interaction is characterized by the Rabi frequency Ω, which is given by the product of the atomic-transition dipole moment and driving-field amplitude. The second and third terms describe the interaction with the two reservoirs and are responsible for spontaneous as well as stimulated emission. The functions $g_c(k)$ and $g_b(k)$ characterize, respectively, the density of cavity and background modes in the cavity. We find it useful to represent the g functions through reservoir response functions. Since the background modes provide an infinitely broad reservoir (with flat spectrum), their response should be immediate. Therefore we postulate for $\tau>0$,

$$\int_0^\infty dk\,|g_b(k)|^2 e^{-i(k-\omega_c)\tau}=\gamma_b\delta(\tau) \ . \quad (7)$$

The coefficient γ_b is a measure of the amount that the background modes contribute to the atomic spontaneous-emission rate. This contribution does not depend on Δ_2. On the other hand, as we have said, the cavity modes describe a finite bandwidth reservoir, i.e.,

$$\int_0^\infty dk\,|g_c(k)|^2 e^{-i(k-\omega_c)\tau}=K(\tau) \ . \quad (8)$$

The function $K(\tau)$ should vanish for $\Gamma\tau\gg1$, where Γ is the cavity resonance width. In the following, we shall consider two particular examples of the cavity-mode response function $K(\tau)$.

For optical cavities, the function $|g_c(k)|^2$ should be of appreciable magnitude only in the frequency range close to a cavity resonance, and we can model $|g_c(k)|^2$ as a simple Lorentzian that peaks at the cavity resonance frequency ω_c and possesses a half width at half maximum of Γ.[34] In such a case,

$$K(\tau)=K_L(\tau)\equiv\gamma_c\Gamma e^{-\Gamma\tau} \ , \quad (9)$$

and, as expected, the reservoir response time is Γ^{-1}. The coefficient γ_c describes the contribution of the cavity modes to the spontaneous-emission rate when $\omega_0=\omega_c$. The total enhanced value of the spontaneous emission rate for $\omega_0=\omega_c$ is therefore

$$\gamma_{\rm tot}=\gamma_c+\gamma_b \ . \quad (10)$$

At this point it should be stressed that for the particular choice of $K(\tau)$ given in Eq. (9), our model can be alternatively described using the quantum Langevin equation[27] or master equation describing the interaction of an atom with a single, damped, cavity mode. If that approach is chosen, the system's dynamics have the appealing property of being Markovian. We prefer, however, to use the approach based on the Hamiltonian description [see Eq. (3)] for the following reasons.

(i) One of our aims will be to eliminate the reservoir's degrees of freedom completely in order to obtain reduced atomic dynamics. Such dynamics will be non-Markovian independently of the choice of $K(\tau)$, provided that the reservoir response time Γ^{-1} is finite.

(ii) The quantum Langevin approach cannot be used if the function $|g_c(k)|^2$ does not have a Lorentzian shape, and, as discussed in the next paragraph, non-Lorentzian shapes are not unknown.

For microwave cavities (wave guides), the appropriate form of the function $|g_c(k)|^2$ is

$$|g_c(k)|^2\propto\Theta(k-\omega_c)\frac{\sqrt{(k-\omega_c)\epsilon}}{k-\omega_c+\epsilon} \ ;$$

for $k-\omega_c\gg\epsilon$ this becomes

$$|g_c(k)|^2\propto\frac{\Theta(k-\omega_c)}{\sqrt{k-\omega_c}} \ , \quad (11)$$

where Θ is a step function and the small constant ϵ smoothens the singularity in the density of modes.[2] In this case, the function $K(\tau)$ can be expressed in terms of some special function; however, for our present purposes, it is sufficient to write a formula for the Laplace transform of the reservoir spectral function

$$\tilde{K}(z)=\int_0^\infty e^{-z\tau}K(\tau)d\tau \ . \quad (12)$$

For microwave cavities we obtain

$$\tilde{K}(z)=\tilde{K}_M(z)\equiv\frac{\gamma_c\sqrt{\epsilon}}{\sqrt{iz}+i\sqrt{\epsilon}} \ , \quad (13)$$

with $\text{Im}(\sqrt{iz})>0$ for $\text{Re}(z)>0$. Note that if the atomic-transition frequency is detuned from the cavity frequency by an amount $\Delta_3\equiv\omega_0-\omega_c>0$, then the cavity modes contribute to the spontaneous-emission rate by an amount

$$\gamma_c(\Delta_3)=\frac{\gamma_c\sqrt{\epsilon\Delta_3}}{\Delta_3+\epsilon}\simeq\gamma_c\left[\frac{\epsilon}{\Delta_3}\right]^{1/2} , \quad (14)$$

where the approximately equal to sign holds when $\Delta_3\gg\epsilon$. Note, however, that this contribution does not diverge at $\Delta_3\to0$, which is a consequence of the smoothing introduced in Eq. (11). Equation (11) suggests that ϵ should be related to the cavity width. The effective cavity width is much larger, however, due to a very slow asymptotic decrease of $\gamma_c(\Delta_3)\propto(\Delta_3)^{-1/2}$ for Δ_3 large and positive.

Having defined the basic features of the model system, we turn our attention to the derivation of the modified Bloch equations, i.e., equations for the mean values of atomic observables. In doing that we shall use the standard Heisenberg-equations approach. We allow for arbitrary values of the effective cavity width Γ, the Rabi frequency Ω and the detunings $\Delta_1=\omega_l-\omega_0$ and $\Delta_2=\omega_l-\omega_c$, except that Γ and Ω are both assumed large compared to γ_c and γ_b. In such a case we may eliminate the photon degrees of freedom by solving Maxwell's equations and substituting the solutions into the Heisenberg equations for the atomic operators. At that point, a Born approximation can be performed which corresponds to a first-order term in a systematic expansion in $\gamma_\nu/\Omega, \gamma_\nu/\Gamma$, where $\nu=c,b$. In performing the Born expansion, one must not, however, perform the Markov approximation, as is usually done when dealing with spontaneous-emission processes in free space.[27] The reason for this lies in the fact that the cavity-mode reservoir has a finite bandwidth which may be comparable with other typical frequency scales such as Ω, Δ_1, or Δ_2.

Let us start by writing a complete set of Heisenberg equations for our system in the rotating frame:

$$\frac{d\hat{\sigma}}{dt}=i\Delta_1\hat{\sigma}+i(\Omega/2)\hat{\sigma}_3+i\int g_b(k)\hat{\sigma}_3\hat{b}_k dk +i\int g_c(k)\hat{\sigma}_3\hat{c}_k dk \ , \tag{14a}$$

$$\frac{d\hat{\sigma}^\dagger}{dt}=-i\Delta_1\hat{\sigma}-i\left[\frac{\Omega}{2}\right]\hat{\sigma}_3-i\int g_c^*(k)\hat{c}_k^\dagger\hat{\sigma}_3 dk -i\int g_b^*(k)\hat{b}_k^\dagger\hat{\sigma}_3 dk \ , \tag{14b}$$

$$\frac{d\hat{\sigma}_3}{dt}=i\Omega(\hat{\sigma}-\hat{\sigma}^\dagger)+2i\int[g_b^*(k)\hat{b}_k^\dagger\hat{\sigma}-g_b(k)\hat{\sigma}^\dagger\hat{b}_k]dk +2i\int[g_c^*(k)\hat{c}_k^\dagger\hat{\sigma}-g_c(k)\hat{\sigma}^\dagger\hat{c}_k]dk \ , \tag{14c}$$

$$\frac{d\hat{c}_k}{dk}=-i(k-\Delta_2)\hat{c}_k-ig_c^*(k)\hat{\sigma} \ , \tag{14d}$$

$$\frac{d\hat{c}_k^\dagger}{dt}=i(k-\Delta_2)\hat{c}_k^\dagger+ig_c(k)\hat{\sigma}^\dagger \ , \tag{14e}$$

$$\frac{d\hat{b}_k}{dt}=-i(k-\Delta_2)\hat{b}_k-ig_b(k)\hat{\sigma} \ , \tag{14f}$$

$$\frac{d\hat{b}_k^\dagger}{dt}=i(k-\Delta_2)\hat{b}_k^\dagger+ig_b(k)\hat{\sigma}^\dagger \ . \tag{14g}$$

The index k enumerating different photons has been chosen so that $k=0$ corresponds to photons of the frequency ω_c in the laboratory frame. The initial state of our system can be assumed to be a tensor product of the atomic ground state and the vacuum states of both photon reservoirs.

The linear Maxwell equations (14d)–(14g) can now be solved and their solution may be inserted into Eqs. (14a)–(14c). Denoting the positive frequency parts of the cavity and background electric fields as

$$\hat{\mathcal{E}}_b^{(+)}(t)=\int g_b(k)\hat{b}_k(t)dk \tag{15a}$$

and

$$\hat{\mathcal{E}}_c^{(+)}(t)=\int g_c(k)\hat{c}_k(t)dk \ , \tag{15b}$$

respectively, and using Eqs. (7) and (8), we obtain

$$\hat{\mathcal{E}}_b^{(+)}(t)=\hat{\mathcal{E}}_{b,\text{free}}^{(+)}-i\gamma_b\hat{\sigma}(t) \ , \tag{16a}$$

$$\hat{\mathcal{E}}_c^{(+)}(t)=\hat{\mathcal{E}}_{c,\text{free}}^{(+)}-i\int_0^t K(t-t')e^{i\Delta_2(t-t')}\hat{\sigma}(t')dt' \ , \tag{16b}$$

where the homogeneous parts $\hat{\mathcal{E}}_{\nu,\text{free}}^{(+)}$ $(\nu=c,b)$ depend only on $\hat{c}_k(0)$ and $\hat{b}_k(0)$, respectively. Inserting the expressions (16a) and (16b) into Eqs. (14a)–(14c), we may perform the quantum-mechanical averaging, making use of normal ordering in Eqs. (14).

The resulting averaged equations contain, however, contributions from two-time atomic correlation functions. For example, the equation for $\langle\hat{\sigma}\rangle=\sigma$ takes the form

$$\frac{d\sigma}{dt}=i\Delta_1\sigma(t)+i\left[\frac{\Omega}{2}\right]\sigma_3(t)-\gamma_b\sigma(t) + \int_0^t K(t-t')e^{i\Delta_2(t-t')}\langle\hat{\sigma}_3(t)\hat{\sigma}(t')\rangle dt' \ . \tag{17}$$

Since $K(t-t')$ is of the first order in γ_c, it is sufficient for lowest-order results to calculate the correlation function in zeroth order (i.e., neglecting both parts of the atom-reservoir interaction). The usual way is then to express two-time correlation functions as linear combinations of one-time averages. If we denote the vector

$$\mathbf{x}=(\sigma,\sigma^\dagger,\sigma_3) \ , \tag{18}$$

the zeroth-order Bloch equations take the form

$$\frac{d\mathbf{x}}{dt}=-G_0\mathbf{x} \ , \tag{19}$$

where the matrix G_0 is

$$G_0=\begin{bmatrix} -i\Delta_1 & 0 & -i\Omega/2 \\ 0 & i\Delta_1 & i\Omega/2 \\ -i\Omega & i\Omega & 0 \end{bmatrix} . \tag{20}$$

Similarly denoting

$$\mathbf{X}_1(t,t')=(\langle\hat{\sigma}(t)\hat{\sigma}(t')\rangle,\langle\hat{\sigma}^\dagger(t)\hat{\sigma}(t')\rangle,\langle\hat{\sigma}_3(t)\hat{\sigma}(t')\rangle) \ , \tag{21}$$

the zeroth-order equations for the correlation functions are

$$\frac{d\mathbf{X}_1}{dt}=-G_0\mathbf{X}_1 \ . \tag{22}$$

The initial conditions for Eqs. (22) are easily stated for $t=t'$. We have then

$$\mathbf{X}_1(t=t',t')=(0,(\sigma_3(t')+1)/2,-\sigma(t')) \ . \tag{23}$$

Quite similarly, one can express the correlation functions

$$\mathbf{X}_2(t,t')=(\langle\hat{\sigma}^\dagger(t')\hat{\sigma}(t)\rangle,\langle\hat{\sigma}^\dagger(t')\hat{\sigma}^\dagger(t)\rangle,\langle\hat{\sigma}^\dagger(t')\hat{\sigma}_3(t)\rangle)$$

through the single-time averages $\mathbf{x}(t')$.

The right-hand side of the Bloch equations will depend then only on the single-time atomic averages, and the dependence will be through typical convolution-type memory integrals.[5] An elegant way to represent them is to use a Laplace transform technique. After a tedious but straightforward calculation, one obtains the Laplace-transformed Bloch equations in the form

$$[z-i\Delta_1+\gamma_\perp(z)]\tilde{\sigma}(z)-i[\Omega-\delta\Omega(z)]\tilde{\sigma}_3(z)/2 =\sigma(0)-i\delta\Omega(z)/2z \ , \quad (24a)$$

$$[z+i\Delta_1+\gamma_\perp^*(z)]\tilde{\sigma}^\dagger(z)+i[\Omega-\delta\Omega^*(z)]\tilde{\sigma}_3(z)/2 =\sigma^\dagger(0)+i\delta\Omega^*(z)/2z \ , \quad (24b)$$

$$[z+\gamma_\parallel(z)]\tilde{\sigma}_3(z)-i[\Omega-\delta\Omega(z)]\tilde{\sigma}(z) +i[\Omega-\delta\Omega^*(z)]\tilde{\sigma}^\dagger(z)=\sigma_3(0)-\gamma_\parallel(z)/z \ . \quad (24c)$$

The z-dependent (in general complex) coefficients $\gamma_\perp(z)$, $\gamma_\perp^*(z)$, and $\gamma_\parallel(z)$ have obvious interpretations as non-Markovian damping rates and radiative (Lamb) shifts of the bare atomic states. Correspondingly, the coefficient $\delta\Omega(z)$ may be interpreted as a non-Markovian radiative shift of the dressed-state energies.

The analytic expressions for the above-discussed coefficients read

$$\gamma_\perp(z)=\gamma_b+\Delta_1^2\frac{\tilde{K}(z-i\Delta_2)}{\Omega'^2} +\frac{\Omega^2[\tilde{K}(z+i\Omega'-i\Delta_2)+\tilde{K}(z-i\Omega'-i\Delta_2)}{2\Omega'^2} \ , \quad (25a)$$

$$\gamma_\perp^*(z)=\gamma_b+\frac{\Delta_1^2\tilde{K}^*(z+i\Delta_2)}{\Omega'^2} +\frac{\Omega^2[\tilde{K}^*(z+i\Omega'+i\Delta_2)+\tilde{K}^*(z-i\Omega'+i\Delta_2)]}{2\Omega'^2} \ , \quad (25b)$$

$$\gamma_\parallel(z)=2\gamma_b+\frac{\Omega^2}{2\Omega'^2}[\tilde{K}(z-i\Delta_2)+\tilde{K}^*(z+i\Delta_2)] +\frac{\Omega^2[\tilde{K}(z+i\Omega'-i\Delta_2)+\tilde{K}^*(z-i\Omega'+i\Delta_2)]}{2(\Omega'-\Delta_1)^2} +\left[\frac{\Omega^2[\tilde{K}(z-i\Omega'-i\Delta_2)+\tilde{K}^*(z+i\Omega'+i\Delta_2)]}{2(\Omega'+\Delta_1)^2}\right] \ , \quad (25c)$$

$$i\delta\Omega(z)=\frac{\Delta_1\Omega\tilde{K}(z-i\Delta_2)}{\Omega'^2} -\frac{\Omega^2}{2\Omega'^2}\left[\frac{\Omega\tilde{K}(z+i\Omega'-i\Delta_2)}{\Omega'-\Delta_1} -\frac{\Omega\tilde{K}(z-i\Omega'-i\Delta_2)}{\Omega'+\Delta_1}\right] \ , \quad (25d)$$

$$-i\delta\Omega^*(z)=\frac{\Delta_1\Omega\tilde{K}^*(z+i\Delta_2)}{\Omega'^2} -\frac{\Omega^2}{2\Omega'^2}\left[\frac{\Omega K^*(z-i\Omega'+i\Delta_2)}{\Omega'-\Delta_1} -\frac{\Omega K^*(z+i\Omega'+\Delta_2)}{\Omega'+\Delta_1}\right] \ , \quad (25e)$$

where

$$\Omega'=(\Omega^2+\Delta_1^2)^{1/2}$$

denotes the dressed-state transition frequency in the absence of interaction with the reservoirs. The above equations may be simplified substantially for particular choices of cavity response (or alternatively spectral functions) and for particular choices of other parameters, such as $\Delta_1=0$ or $\Delta_2=0$ (see Sec. IV).

We remind the reader of the two spectral functions discussed earlier. For optical cavities with Lorentzian line shape, we have

$$K_L(z)=K_L^*(z)=\frac{\gamma_c\Gamma}{\Gamma+z} \ . \quad (26a)$$

On the other hand, for microwave cavities (wave guides) close to their fundamental frequency, we obtain

$$K_M(z)=\frac{\gamma_c\sqrt{\epsilon}}{\sqrt{iz}+i\sqrt{\epsilon}} \quad \text{with } \mathrm{Im}(\sqrt{iz}\,)\geq 0 \quad \text{for } \mathrm{Re}(z)\geq 0 \ , \quad (26b)$$

$$K_M^*(z)=\frac{\gamma_c\sqrt{\epsilon}}{\sqrt{-iz}-i\sqrt{\epsilon}} \quad \text{with } \mathrm{Im}(\sqrt{-iz}\,)\leq 0 \quad \text{for } \mathrm{Re}(z)\geq 0 \ . \quad (26c)$$

The modified Bloch equations (24) together with Eqs. (25) are the main results of this section. We shall end this section making a few general comments on the form of Eqs. (24).

(i) These equations are valid only in the sense of the Born expansion in γ_c and γ_b. Strictly speaking, they are reliable only up to terms of the order $(\gamma_\nu/\Omega)^2$ or $(\gamma_\nu/\Gamma)^2$, where $\nu=b,c$. Higher-order correction may be, however, calculated in the course of a systematic expansion. The explicit calculation of the single-time mean values is described in the Appendix. Higher-order corrections are included simply by breaking down the hierarchy of the equations for one single-time correlation function at a sufficiently high level.

(ii) Equations (24) contain the usual (Markovian) contribution from the background modes.

(iii) Terms associated with the cavity modes have characteristic convolution-type memory integrals in the time domain (z dependence in the Laplace-transformed picture). The memory extends over the cavity response time Γ^{-1} for the Lorentzian cavity line shapes, Eq. (9). The memory has a long-time algebraic tail for the nonsymmetric nonanalytical cavity line shapes such as described in Eq. (11).

(iv) In the limit $\Gamma\gg\Omega,\gamma_c$ and for Lorentzian cavity response, Eqs. (24) reduce to the usual Bloch equations with $\gamma_s = \gamma_b + \gamma_c$ [see Eq. (10)].

(v) For the wave-guide case [Eq. (11)], the usual Bloch limit can be also found, but it requires a more complicated set of conditions. Namely, ϵ must be large and Δ_2 must be of the same order. Also it is necessary that $\Omega, \Delta_1 \ll \epsilon$. The latter conditions follow from the fact that the density of photon modes [see Eq. (11)] has a maximum at $k - \omega_c \simeq \epsilon$, which is close to zero for small ϵ but shifts towards the violet when ϵ grows. This limit, however, does not interest us, since in fact the main motivation for introducing Eq. (11) is to study the drastic departures from the usual Bloch-type behavior.

IV. POWER SPECTRA OF FLUORESCENCE

The power spectrum of the fluorescent light is given by the well-known formula

$$S_\nu(\omega) = \lim_{t\to\infty} \mathrm{Re} \int_0^\infty e^{i\omega\tau} \langle \hat{\mathcal{E}}_\nu^{(-)}(t+\tau) \hat{\mathcal{E}}_\nu^{(+)}(t) \rangle d\tau \;, \tag{27}$$

where $\nu = b$ or c, depending on which of the fields is detected. Equation (27) relates the spectrum to the Laplace transform of the stationary field-autocorrelation function and can be evaluated in terms of atomic-autocorrelation functions. However, since the reduced atomic dynamics are non-Markovian and the quantum regression theorem does not hold, the equations for the atomic-autocorrelation functions have a form different from the Bloch equations [Eq. (24)] and must be derived separately. This additional exercise can be avoided if one makes use of the identity[35]

$$S_\nu(k) = \lim_{T\to\infty} \frac{1}{2T} \langle \hat{\mathcal{E}}_\nu^{(-)}(k,T) \hat{\mathcal{E}}_\nu^{(+)}(k,T) \rangle \;, \tag{28}$$

where

$$\hat{\mathcal{E}}_\nu^{(\pm)}(k,T) = \int_0^T e^{\pm ikt'} \hat{\mathcal{E}}_\nu^{(\pm)}(t') dt' \;.$$

By direct inspection, one can then show that, in fact,

$$S_c(k) = \lim_{T\to\infty} \frac{1}{2T} \langle \hat{c}^\dagger_{k+\Delta_2}(T) \hat{c}_{k+\Delta_2}(T) \rangle \;, \tag{29a}$$

$$S_b(k) = \lim_{T\to\infty} \frac{1}{2T} \langle \hat{b}^\dagger_{k+\Delta_2}(T) \hat{b}_{k+\Delta_2}(T) \rangle \;. \tag{29b}$$

Equation (29) expresses the power spectrum in terms of a single-time mean value. Using the Maxwell equations (14d)–(14g), we immediately find the "optical theorem"

$$S_c(k) = -\,\mathrm{Im}[\lim_{z\to 0} z\, g_c(k+\Delta_2) \langle \hat{\sigma}^\dagger \hat{c}_{k+\Delta_2} \rangle] \;, \tag{30a}$$

$$S_b(k) = -\,\mathrm{Im}[\lim_{z\to 0} z\, g_b(k+\Delta_2) \langle \hat{\sigma}^\dagger \hat{b}_{k+\Delta_2} \rangle] \;. \tag{30b}$$

Denoting

$$\mathbf{x}(t) = (\sigma(t), \sigma^\dagger(t), \sigma_3(t)) \;,$$

the modified Bloch equations (24) can be written in the Laplace-transformed matrix form

$$\tilde{G}(z)\tilde{\mathbf{x}}(z) = \mathbf{x}(0) + \tilde{\mathbf{R}}(z) \;, \tag{31}$$

where $\tilde{\mathbf{R}}$ is a vector giving rise to the inhomogeneous terms on the right-hand side of Eqs. (24). A calculation similar to the one discussed in Sec. III allows us to derive the equations fulfilled by the vectors

$$\mathbf{Y}_c(t) = (\langle \hat{\sigma}\hat{c}_k(t) \rangle, \langle \hat{\sigma}^\dagger \hat{c}_k(t) \rangle, \langle \hat{\sigma}_3 \hat{c}_k(t) \rangle) \;, \tag{32a}$$

$$\mathbf{Y}_b(t) = (\langle \hat{\sigma}\hat{b}_k(t) \rangle, \langle \hat{\sigma}^\dagger \hat{b}_k(t) \rangle, \langle \hat{\sigma}_3 \hat{b}_k(t) \rangle) \;. \tag{32b}$$

In Laplace-transformed form, the equations read

$$\tilde{G}[z + i(k-\Delta_2)]\tilde{\mathbf{Y}}_\nu(z) = -ig_\nu^*(k) \left[\tilde{\mathbf{T}}(z) + \frac{\tilde{R}[z + i(k-\Delta_2)]\tilde{\sigma}(z)}{z + i(k-\Delta_2)} \right] \;, \tag{32c}$$

where the vector $\tilde{T}(z)$ is given by

$$\tilde{\mathbf{T}}(z) = \begin{bmatrix} 0 \\ [\tilde{\sigma}_3(z) + 1/z]/2 \\ -\tilde{\sigma}(z) \end{bmatrix} \;. \tag{33}$$

A direct calculation of the $z \to 0$ limit in Eq. (30) leads to the final expressions for the spectra. They are

$$S_c(k) = \mathrm{Re} \left[|g_c(k+\Delta_2)|^2 \sum_{i=1}^{3} \tilde{G}_{2i}^{-1}(ik) \left[\frac{\delta_{i2}(\sigma_{3\mathrm{st}}+1)}{2} - \delta_{i3}\sigma_{\mathrm{st}} + \tilde{R}_i(ik)\sigma_{\mathrm{st}} \right] \right] \;, \tag{34}$$

$$S_b(k) = \frac{\gamma_b}{|g_c(k+\Delta_2)|^2} S_b(k) \;. \tag{35}$$

Here the subscript st denotes stationary values of the atomic moments obtained from Eq. (31), i.e.,

$$\lim_{t\to\infty} \mathbf{x}(t) = \mathbf{x}_{\mathrm{st}} = \lim_{z\to 0} [G^{-1}(z)\tilde{\mathbf{R}}(z)z] \;. \tag{36}$$

Equations (34) and (35) exhibit two important properties.

(i) The cavity-mode spectrum contains the density-of-modes factor $|g_c(k+\Delta)|^2$. This factor accounts for the direct effect of the photon-mode density on the spectrum. For example, in the case of a Lorentzian cavity line shape and with the laser, atom, and cavity all resonant, this factor leads (for $\Omega \gg \Gamma$) to a suppression of the amplitude of the spectral sidebands. Such suppression has a "passive" character and can be easily predicted. It is much more difficult to predict the dynamical narrowing or broadening of the peaks in the spectrum.

(ii) The spectrum of the background modes does not contain the factor $|g_c(k+\Delta)|^2$. This feature follows from the fact that the density of the background modes is constant in the frequency range of interest.

For the next few paragraphs we will concentrate on the situation in which the cavity profile is Lorentzian [Eq. (8)] and the atomic and laser frequencies coincide ($\Delta_1=0$). In this case the equations are simple enough to discuss analytically, at least for large Ω. Let us first look at the Bloch equations (24). In the limit of strong excitation ($\Omega \gg \gamma_b, \gamma_c$), the dressed-state description[36] is particularly convenient. In the case $\Delta_1=0$, the population inversion of the dressed states is equal to the σ_1 component of the Bloch vector.[25,26] In the lowest order in γ_v/Ω and γ_v/Γ, $\sigma_1(t)$ behaves as

$$\sigma_1(t)=e^{-\gamma(\Omega)t}[\sigma_1(0)+\sigma_{1,\mathrm{st}}(\Omega)(e^{\gamma(\Omega)t}-1)] . \tag{37}$$

The decay constant is given by the formula

$$\begin{aligned}\gamma(\Omega)&=\left[\frac{\gamma_\perp(0)+\gamma_\perp^*(0)}{2}\right]\\ &=\gamma_b+\frac{\gamma_c}{2}\left[\frac{\Gamma^2}{\Gamma^2+(\Omega-\Delta_2)^2}+\frac{\Gamma^2}{\Gamma^2+(\Omega+\Delta_2)^2}\right],\end{aligned} \tag{38}$$

whereas the stationary value of σ_1 is

$$\begin{aligned}\sigma_{1,\mathrm{st}}&=-\frac{i[\delta\Omega(0)-\delta\Omega^*(0)]}{2\gamma(\Omega)}\\ &=\frac{\gamma_c}{2\gamma(\Omega)}\left[\frac{\Gamma^2}{\Gamma^2+(\Omega-\Delta_2)^2}-\frac{\Gamma^2}{\Gamma^2+(\Omega+\Delta_2)^2}\right].\end{aligned} \tag{39}$$

Equations (38) and (39) have a very simple physical interpretation. The decay constant $\gamma(\Omega)$ is bounded from below by the contribution from the background modes γ_b (which may in principle be very small, much smaller than the spontaneous-emission rate in free space). The damping constant is substantially affected by the cavity modes contribution if and only if the Rabi frequency shifts the frequency of the sidebands close to the center of the cavity line. In mathematical terms, $|\Omega+\Delta_2|$ or $|\Omega-\Delta_2|$ have to be smaller than the cavity width Γ. Obviously, by changing Ω, we may dynamically suppress or enhance the rate $\gamma(\Omega)$. For $\Delta_2=0$, $\gamma(\Omega)$ will decrease from the value $\gamma_c+\gamma_b$ (for $\Omega \ll \Gamma$) to γ_b (for $\Omega \gg \Gamma$).[5] Similarly, for $\Delta_2 \gg \Gamma$, we may encounter a situation in which $\gamma(\Omega)$ will grow from the value γ_b (for $\Omega \ll \Gamma$) to $\gamma_b+\gamma_c/2$ (for $|\Omega-\Delta_2| \ll \Gamma$), and then decrease to the value γ_b for $\Omega \to \infty$.

The dressed-state population inversion is obviously zero for $\Delta_2=0$. However, as soon as $\Delta_2 \neq 0$, the densities of the photon states corresponding to sideband frequencies $\omega_l \pm \Omega$ are different. For positive Δ_2, the density of the cavity modes is larger at $\omega_l-\Omega$. That means that the transition from lower to upper dressed states should be more efficient than the transition from the upper to the lower dressed state (at $\omega_l+\Omega$). In effect, in the stationary limit, the lower dressed state should be less populated ($\sigma_1>0$). As we see from Eq. (39), it is indeed the case. The inversion of the dressed-state population is, in fact, proportional to the difference of photon-mode densities at $\omega_l-\Omega$ and $\omega_l+\Omega$. This result implies that a *high Q* cavity can be employed to maintain a *large steady-state inversion* of the dressed-state levels *even* in the case of *zero atom-laser detuning.*

Similar analysis shows that the dressed-state polarization

$$\sigma_{+-}=(\sigma_2+i\sigma_3)/2$$

behaves as

$$\sigma_{+-}(t)=e^{-[\gamma'(\Omega)+i\Omega'(\Omega)]t}[\sigma_{+-}(0)+\sigma_{+-,\mathrm{st}}(e^{[\gamma'(\Omega)+i\Omega'(\Omega)]t}-1)] , \tag{40}$$

where $\gamma'(\Omega)$ and $\Omega'(\Omega)$ are defined as the real and imaginary parts of

$$\lambda(\Omega)=\left[\frac{\gamma_\perp(z)+\gamma_\perp^*(z)}{4}+\frac{\gamma_\parallel(z)}{2}+i\left[\Omega-\frac{\delta\Omega(z)+\delta\Omega^*(z)}{2}\right]\right]_{z=-i\Omega}, \tag{41}$$

respectively. Explicit calculation gives

$$\gamma'(\Omega)=\frac{3\gamma_b}{2}+\frac{\gamma_c\Gamma^2}{\Gamma^2+\Delta_2^2}+\frac{\gamma_c\Gamma^2}{4[\Gamma^2+(\Omega-\Delta_2)^2]}+\frac{\gamma_c\Gamma^2}{4[\Gamma^2+(\Omega+\Delta_2)^2]} , \tag{42}$$

$$\Omega'(\Omega)=\Omega+\frac{\gamma_c(\Omega-\Delta_2)\Gamma}{4[\Gamma^2+(\Omega-\Delta_2)^2]}+\frac{\gamma_c(\Omega+\Delta_2)}{4[\Gamma^2+(\Omega+\Delta_2)^2]} . \tag{43}$$

Note that $\gamma'(\Omega)$ is the width of the sidebands in the fluorescence power spectrum. As we see from Eq. (42), it too gets dynamically suppressed or enhanced, depending on the value of Ω. Equation (43) indicates that the position of the sidebands is shifted and that the shift changes sign for $\Omega \simeq |\Delta_2|$.

The above analysis indicates that the fluorescence into the background modes should have a spectrum consisting of three Lorentzian peaks. The central peak has a width as given by Eq. (38) and height $\simeq(1-\sigma_{1,\mathrm{st}}^2)/\gamma(\Omega)$. If the stationary value of the dressed-state inversion is close to ± 1, the central peak height becomes small. This is a rather striking and novel effect. The conventional dressed-state theory applied to strong-field-induced resonance scattering predicts that the height of the central peak is equal to the sum of the populations of the dressed states divided by the decay rate of the σ_1 component of the Bloch vector. This statement is true, however, only in free space, when the stationary value of $\sigma_{1,\mathrm{st}}$ equals zero and σ_1 does not contribute to elastic scattering, which, in fact, is negligibly weak for large Ω. If $\sigma_{1,\mathrm{st}}$ does not equal zero, σ_1 contributes to an elastic component of the spectrum by an amount $\sigma_{1,\mathrm{st}}^2\delta(k-\omega_l)$. The additional suppression of the central peak height in the present inelastic spectrum stems the fact that a significant part of the photons will be scattered elastically. Similarly, the sidebands will have a width given by Eq. (42) and will be shifted by $\Omega'(\Omega)-\Omega$ [see Eq. (43)]. The heights of the sidebands can be roughly estimated to be proportional to the stationary values of the dressed-state populations,

$$h_{\mathrm{left}} \simeq (1-\sigma_{1,\mathrm{st}})/2\gamma'(\Omega) ,$$
$$h_{\mathrm{right}} \simeq (1+\sigma_{1,\mathrm{st}})/2\gamma'(\Omega) . \tag{44}$$

The results of our discussion of Lorentzian cavity line shape and zero atom-laser detuning are illustrated in Figs. 1–3. We present there the Ω dependence of the background-mode spectrum for the case of $\Delta_2=5\Gamma$. Figures 2(a)–2(c) show the detailed behavior of the central and sideband peaks shown in Fig. 1. Note the radiative frequency shifts of the sidebands. Finally, Fig. 3 compares the peak widths and heights for $\Omega=\Delta_2$.

We comment briefly on the requirements that must be satisfied before one would expect to experimentally observe the features predicted in Figs. 1–3. First of all, our calculations are valid only in regimes in which $\gamma_v/\Gamma \ll 1$ and $\gamma_v/\Omega \ll 1$, where $v=b,c$. Additionally, the most interesting effects occur when $\Omega > \Gamma$. Finally, in order for the effects to be significant, we must have γ_c at least comparable to γ_b. The latter condition can be satisfied in confocal optical resonators[4] constructed with spherical mirrors having radii on the order of millimeters, provided that a finesse on the order of 100 can be achieved.

Obviously, the analytical treatment discussed above is valid only if $\Omega,\Gamma \gg \gamma_c,\gamma_b$. We should stress that Eq. (34) contains much more information. The spectrum even for Lorentzian cavity line shapes does not consist strictly speaking of Lorentzian peaks, due to a non-Markovian z dependence in Eq. (34).

We now consider spectra under more general conditions, beginning with a discussion of spectra in the presence of non-Lorentzian cavity line shapes but still assuming that the atom-laser detuning is zero. The non-Markovian effects referred to in the previous paragraph are especially visible in such cases. For wave-guide-like mode densities [see Eq. (11)], the approximate formulas (37) or (40) will be valid only in certain frequency regions. Decay processes may be nonexponential, especially if any

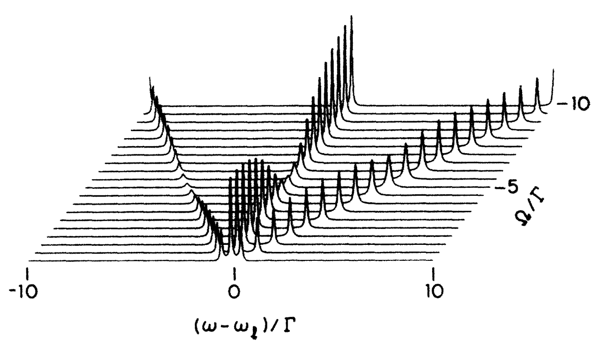

FIG. 1. Spectrum of resonance fluorescence emitted by atoms confined in a detuned cavity and resonantly driven as a function of driving-field Rabi frequency. These spectra correspond to light emitted into background modes (i.e., out the sides of the cavity). Horizontal, frequency (increasing to the right); vertical, relative fluorescence intensity. Successive traces correspond to increasing Rabi frequency. In this figure, and Figs. 2 and 3, $\gamma_b/\Gamma=0.03$, $\gamma_c/\Gamma=0.2$, the laser-atom detuning $\Delta_1=0$, and the laser-cavity detuning $\Delta_2=5\Gamma$. Note that when $\Omega\simeq\Delta_2$, the lower-frequency sideband becomes resonant with the cavity. This resonance results in a polarization of the dressed-state population and a concomitant drop in the intensity of the fluorescence emitted on the lower sideband into the background modes. Note that the central peak simultaneously exhibits a strong attenuation. See the text for a discussion of this novel effect.

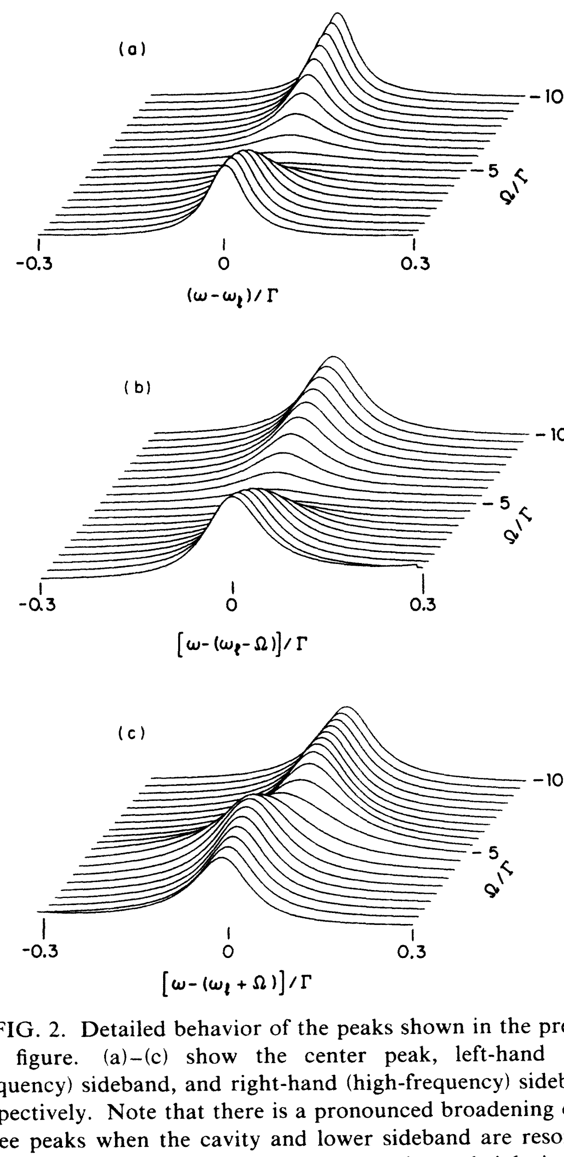

FIG. 2. Detailed behavior of the peaks shown in the preceding figure. (a)–(c) show the center peak, left-hand (low-frequency) sideband, and right-hand (high-frequency) sideband, respectively. Note that there is a pronounced broadening of all three peaks when the cavity and lower sideband are resonant. The peaks are normalized to the same maximum height in each part of the figure so that relative heights must be ascertained from Fig. 1.

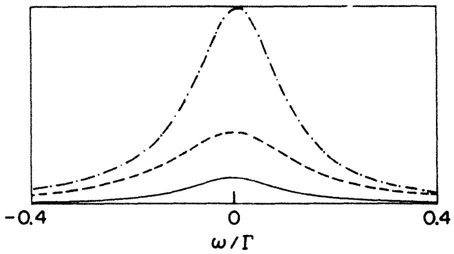

FIG. 3. Close-up view of the three peaks in Fig. 1 for $\Omega=5\Gamma=\Delta_2$. The dashed, solid, and dashed-dotted traces correspond to the center, left, and right peaks, respectively. All three peaks are plotted on the same vertical and horizontal scales. With $\Omega=\Delta_2$, the lower fluorescent sideband (solid trace) is resonant with the cavity. The selective dressed-state depletion that results polarizes the dressed-state populations, thereby modifying the relative heights of the fluorescence peaks—even though the peaks shown correspond to emission into the background modes (See Fig. 1). In this figure, the sidebands have been displaced toward the central peak by the Rabi frequency.

of the characteristic frequencies ω_l, $\omega_l \pm \Omega$ are close to the threshold frequency ω_c. Spectra obtained using Eq. (11) are related to those studied in the context of near-threshold ionization.[37] Figures 4–6 illustrate this point by showing an overall view of the spectrum, detailed pictures of the peaks Ω dependence, and shape of the peaks for $\Omega \simeq \Delta_2$, respectively. The threshold effects lead to the strong modifications of the peak shapes.

Finally, Figs. 7–9 illustrate the case of the Lorentzian cavity line shape, but with a nonzero value of the atom-cavity detuning. The physics here is essentially the same though technically more difficult to describe analytically.

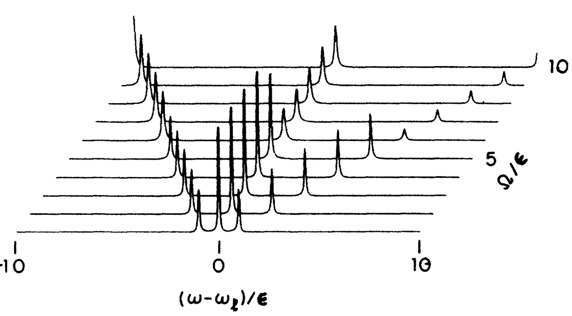

FIG. 4. Spectrum of resonance fluorescence emitted by resonantly driven atoms in a cavity having a photon-mode density described by Eq. (11). The spectra are associated with emission out the sides of the cavity. Axes are as described in Fig. 1. In this figure and Figs. 5 and 6 the laser-atom detuning, $\Delta_1=0$, the cavity-atom detuning $\Delta_2 \equiv \omega_c-\omega_0=-5\epsilon$, $\gamma_b=0.03\epsilon$, and $\gamma_c=0.2\epsilon$. With $\Delta_2=-5\epsilon$, the atom-cavity coupling turns on abruptly when $\Omega=|\Delta_2|$ as the upper sideband moves into the spectral region of high cavity-mode density. For $\Omega<|\Delta_2|$, an essentially normal Mollow spectrum is observed. For $\Omega>|\Delta_2|$, the dressed-state populations are polarized and the spectrum becomes asymmetric.

V. SQUEEZING SPECTRUM OF THE FLUORESCENT LIGHT

As we have mentioned in the Introduction, cavity atoms may experience significant squeezing under the influence of the strong driving field.[16] These squeezing effects are intrinsically connected to the polarization of the dressed-state population which was discussed in Sec. IV. According to Eq. (39), by tuning the cavity appropriately (close to $\omega_l \pm \Omega$), we may induce a nonvanishing inversion of the dressed states ($\sigma_1 \neq 0$). This statement remains true even if $\Delta_1 \neq 0$. At the same time, especially for $\Delta_1 \neq 0$, the bare-state inversion σ_3 may remain different from zero. These are optimal conditions for atomic squeezing.

Unfortunately, as we shall show here, quite large atomic-squeezing effects do not lead to large squeezing of the fluorescent light. It is a purpose of this part of the present paper to examine the squeezing properties of the

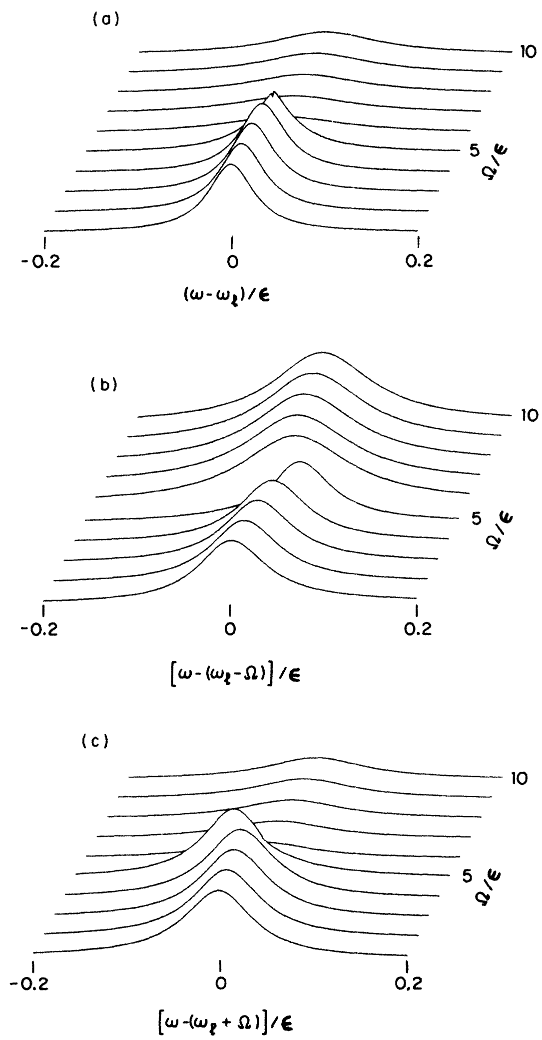

FIG. 5. Detailed behavior of the peaks shown in Fig. 4. (a)–(c) show the center peak, left-hand (low-frequency), and right-hand (high-frequency) sidebands, respectively. Note the abrupt change in character of the peaks as the upper sideband moves into the region of high cavity-mode density.

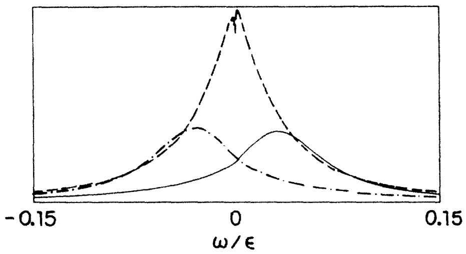

FIG. 6. Close-up view of the peaks in Fig. 4 for the special case of $\Omega = |\Delta_2|$. The dashed, solid, and dashed-dotted traces correspond to the center, left, and right peaks, respectively. All three peaks are plotted on the same vertical and horizontal scales. With $\Omega = |\Delta_2|$, the sharp edge of the cavity-mode-density function coincides with the upper sideband, giving the fluorescent peaks a strong non-Lorentzian character. At this particular Rabi frequency, the central peak displays an interesting narrow dip at its center. The dip results because of the abrupt change in cavity-mode density coincident with one of the characteristic fluorescence frequencies. The details of the dip are model dependent, but it should occur quite generally when a discontinuity in the reservoir mode density coincides with a characteristic emission frequency.

scattered radiation. Because of the Markovian nature of the background photon modes, radiation scattered into them is directly related to the instantaneous atomic dipole moment. However, under the assumption $\gamma_b \ll \gamma_c$, only a small fraction of the photons are scattered into the background modes. The field scattered into the cavity modes at time t is, on the other hand, related to the sum of atomic contributions coming from different times between $(t, t-\Gamma^{-1})$. Different terms in such a sum may interfere destructively, destroying squeezing properties.

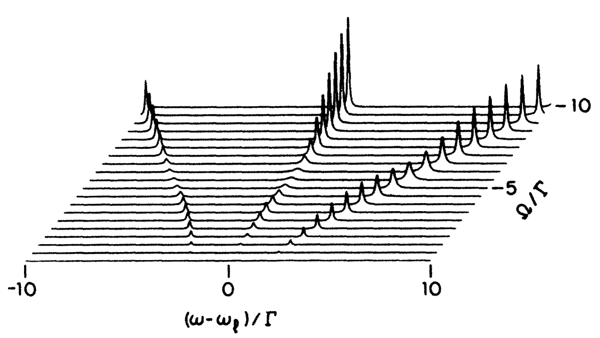

FIG. 7. Spectrum of resonance fluorescence emitted by atoms confined within a detuned cavity and exposed to a detuned driving field as a function of driving-field Rabi frequency. See Fig. 1 for a description of the axes. Spectra shown correspond to emission into the background modes of the cavity. In this figure, as well as in Figs. 8 and 9, the laser-atom detuning $\Delta_1 = 2\Gamma$ and the laser-cavity detuning $\Delta_2 = 6\Gamma$. Also, $\gamma_b/\Gamma = 0.03$ and $\gamma_c/\Gamma = 0.2$. As seen in Fig. 1, when the cavity is resonant with the lower sideband, both the lower sideband and the center peak are suppressed. The principle effect on the spectra of introducing a nonzero atom-laser detuning appears to be the suppression of the fluorescence peaks for $\Omega < \Delta_2$.

In order to study this question we have calculated the quantities that characterize the squeezing of the scattered field. One possibility is to calculate the relative variance of the total field. Such a variance would be normalized with respect to the value it attains in the absence of interaction in the usual vacuum or coherent state. The normalization constant is infinite in free space since the photons of all frequencies contribute equally to it. The total-field variance is, by definition, unity in free space but may drop below 1 for finite bandwidth fields like those found in optical cavities. It generally remains quite close to unit, however, and in our case the dip below unity amounts to 1% or 2% squeezing. Much more detailed information can be obtained by studying the spectrum of squeezing[38] rather than the total-field variance. This quantity is directly measurable in schemes involving homodyne or heterodyne detection and gives information

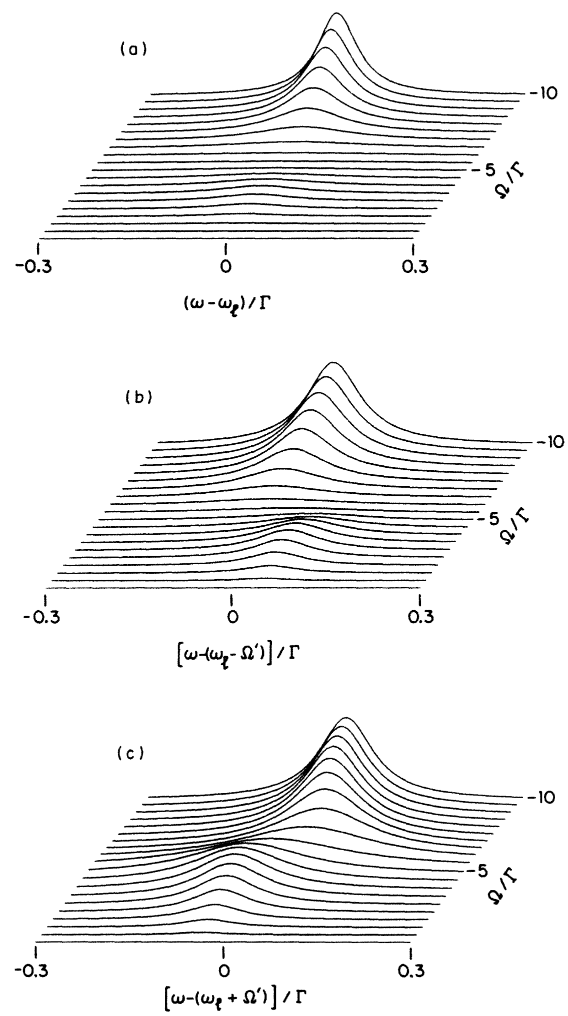

FIG. 8. Detailed behavior of the peaks shown in Fig. 7. (a)–(c) show the center peak, left-hand (low-frequency) sideband, and right-hand (high-frequency) sideband, respectively. Interesting broadening and shifts of the peaks can be seen when the lower sideband is resonant with the cavity. The peaks are normalized to the same maximum height in each part of this figure so the relative heights of the various peaks must be ascertained from Fig. 7.

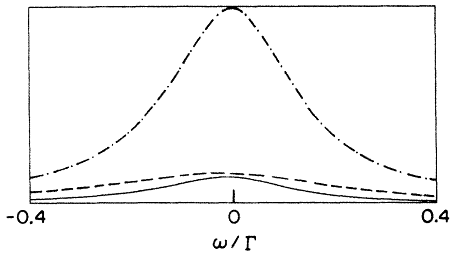

FIG. 9. Close-up view of the three peaks in Fig. 7 for $\Omega=5.66\Gamma$ (i.e., $\Omega'=\Delta_2$). The dashed, solid, and dashed-dotted traces correspond to the center, left, and right peaks, respectively. All three peaks are plotted on the same vertical and horizontal scales. With $\Omega=5.66\Gamma$, the lower fluorescent sideband (solid trace) is resonant with the cavity and polarization of the dressed-state population occurs. In this figure, the sidebands have been displaced toward the center by the generalized Rabi frequency.

about relative squeezing of the field at particular photon frequencies ω.

The spectrum of squeezing is defined as the Laplace transform of the corresponding electric field component normally and time-ordered autocorrelation function. Defining

$$\mathcal{E}_\phi(t)=\hat{\mathcal{E}}^{(-)}(t)e^{i\phi}+\hat{\mathcal{E}}^{(+)}(t)e^{-i\phi}\ , \tag{45}$$

we have

$$Q_\phi(\omega)=\lim_{t\to\infty}\operatorname{Re}\int_0^\infty \langle :\hat{\mathcal{E}}_\phi(t+\tau)\hat{\mathcal{E}}_\phi(t): \rangle e^{-i\omega\tau}d\tau\ . \tag{46}$$

We normalize this spectrum to the value it has in the absence of both interaction and normal ordering,

$$N(\omega)=\lim_{t\to\infty}\operatorname{Re}\int_0^\infty \langle \hat{\mathcal{E}}^{(-)}_{\phi,\mathrm{free}}(t+\tau)\hat{\mathcal{E}}^{(+)}_{\phi,\mathrm{free}}(t)\rangle e^{-i\omega\tau}d\tau\ . \tag{47}$$

The spectrum so defined is greater than -1 and shows relative squeezing if it becomes smaller than 0. In our present model, the component of the scattered electric field which is induced by the σ_1 component of the atomic dipole moment corresponds to $\phi=\pi/2$. We shall consider only this case in the following and skip the index ϕ. Also we discuss squeezing of the background and cavity modes separately and denote the corresponding squeezing spectra $Q_b(\omega)$ and $Q_c(\omega)$, respectively.

Both spectra can be derived from Eq. (46) after deriving and solving the equations for normally and time-ordered correlation functions. For example, assuming a Lorentzian cavity line shape, the Laplace transform of the stationary correlation function

$$c(\tau)=\lim_{t\to\infty}\mathcal{E}_c^{(+)}(t+\tau)\mathcal{E}_c^{(+)}(\tau)$$

fulfills

$$(z+\Gamma-i\Delta_2)\tilde{c}(z)=\langle \hat{\mathcal{E}}_c^{(+)2}\rangle_{\mathrm{st}}-i\frac{\gamma_c\Gamma}{2}\tilde{V}_1(z)\ , \tag{48}$$

where $\tilde{V}_1(z)$ is the first component of the vector $\tilde{\mathbf{V}}$ which is comprised of Laplace transforms of correlation functions

$$\mathbf{V}(\tau)=\lim_{t\to\infty}[\langle\hat{\sigma}(t+\tau)\hat{\mathcal{E}}_c^{(+)}(t)\rangle,\langle\hat{\sigma}^\dagger(t+\tau)\hat{\mathcal{E}}_c^{(+)}(t)\rangle,\langle\hat{\sigma}_3(t+\tau)\hat{\mathcal{E}}_c^{(+)}(t)\rangle]\ . \tag{49}$$

Calculations similar to the ones discussed in Sec. III lead to the result

$$\tilde{G}(z)\tilde{\mathbf{V}}(z)=\mathbf{Y}_{\mathrm{st}}+\tilde{\mathbf{R}}(z)\mathcal{E}^{(+)}_{c,\mathrm{st}}+\tilde{\mathbf{P}}(z)\ , \tag{50}$$

where the vector $\tilde{\mathbf{P}}(z)$ is given by

$$\tilde{\mathbf{P}}(z)=iM(z+\Gamma+G_0-i\Delta_2)^{-1}\begin{bmatrix}\langle\hat{\sigma}(\hat{\mathcal{E}}_c^{(+)})^2\rangle_{\mathrm{st}}\\ \langle\hat{\sigma}^\dagger(\hat{\mathcal{E}}_c^{(+)})^2\rangle_{\mathrm{st}}\\ \langle\hat{\sigma}_3(\hat{\mathcal{E}}_c^{(+)})^2\rangle_{\mathrm{st}}\end{bmatrix}$$
$$-iM^*(z+\Gamma+G_0^*+i\Delta_2)^{-1}\begin{bmatrix}\langle\hat{\mathcal{E}}_c^{(-)}\hat{\sigma}\hat{\mathcal{E}}_c^{(+)}\rangle_{\mathrm{st}}\\ \langle\hat{\mathcal{E}}_c^{(-)}\hat{\sigma}^\dagger\hat{\mathcal{E}}_c^{(+)}\rangle_{\mathrm{st}}\\ \langle\hat{\mathcal{E}}_c^{(-)}\hat{\sigma}_3\hat{\mathcal{E}}_c^{(+)}\rangle_{\mathrm{st}}\end{bmatrix}\ , \tag{51}$$

while the matrices M,M^* are

$$M=\begin{bmatrix}0&0&1\\0&0&0\\0&-2&0\end{bmatrix}$$

and

$$M^*=\begin{bmatrix}0&0&0\\0&0&1\\-2&0&0\end{bmatrix}\ .$$

The matrix G_0 is defined by Eq. (20), $\mathbf{R}(z)$ by Eq. (31), and $\tilde{\mathbf{Y}}(z)$ by Eq. (32a). For the evaluation of the single-time stationary values such as $\langle\hat{\mathcal{E}}_c^{(-)}\hat{\sigma}\hat{\mathcal{E}}_c^{(+)}\rangle_{\mathrm{st}}$ see the Appendix.

The results of our calçulations may be summarized as follows.

(a) The squeezing spectrum of the background field does not show as much squeezing as one would expect from the fact that the final atomic state is strongly squeezed. The quantitative reason for this is that, in the limit of interest when $\gamma_b \ll \gamma_c$, only a fraction (roughly γ_b/γ_c) is scattered into the background modes. This results in suppression of the maximal squeezing.

(b) The squeezing spectrum of the cavity radiation which is normalized with respect to the constant density of outgoing modes shows maximal squeezing of the same order as one would obtain in free-space resonance fluorescence (i.e., $\simeq 16\%$). However, it should be stressed that such squeezing is obtained in regimes that do not show any squeezing in the free-space case. An example is

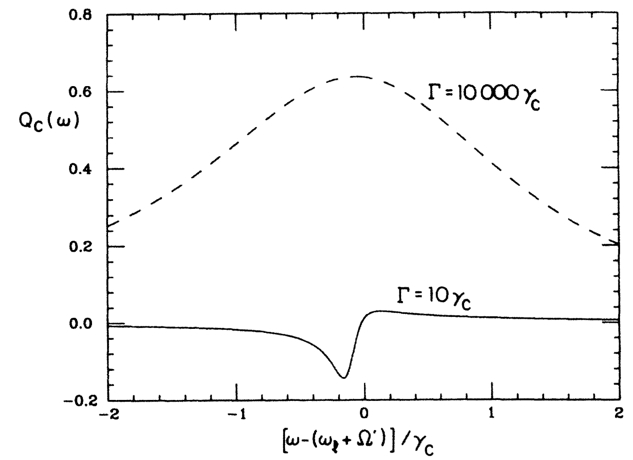

FIG. 10. Spectrum of squeezing near the Rabi sideband of atoms in a cavity (solid line) and in free space (dashed line). As indicated, the free-space result is obtained by letting Γ become very large. Negative values of $Q_c(\omega)$ indicate the presence of squeezing. In this figure, $\Delta_1=5\gamma_c$, $\Delta_2=50\gamma_c$, $\Omega=30\gamma_c$, and $\gamma_b=0.01\gamma_c$. This spectrum corresponds to light emitted into cavity modes.

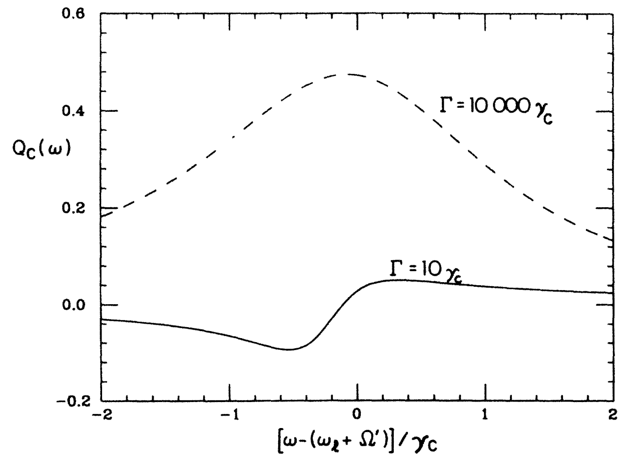

FIG. 11. Spectrum of squeezing near the Rabi sideband of atoms in a cavity (solid line) and in free space (dashed line). Parameter values have been chosen by trial and error to maximize the magnitude and bandwidth of the squeezing. In this figure, $\Delta_1=10\gamma_c$, $\Delta_2=30\gamma_c$, $\Omega=20\gamma_c$, and $\gamma_b=0.01\gamma_c$.

shown in Fig. 10. In free space, this corresponds to strong-field, nearly resonant, excitation and no squeezing. In the cavity, narrow-band squeezing effects are observed at the frequencies close to the Mollow sidebands. Another example is presented in Fig. 11, which corresponds to the choice of parameters maximizing relative atomic squeezing and polarization of the dressed states.[16]

Summarizing, we have shown that by using carefully designed cavities (such that $\gamma_b \ll \gamma_c$), squeezing effects significantly different from those in free space may be produced via strong-field excitation of cavity-contained two-level atoms.

ACKNOWLEDGMENTS

We thank R. J. Glauber for enlightening conversations concerning the topics discussed here, and we acknowledge the financial support of the National Science Foundation, Grant No. PHY85-04260 and the U.S. Office of Naval Research, Grant No. N00014-85-K-0724.

APPENDIX

In this appendix we shall discuss in detail the method of obtaining higher-order results. We shall construct the hierarchy of equations for one-time normally ordered correlation functions. For Lorentzian cavity line shape, the easiest way to do it uses the quantum Langevin equation for the cavity field[27]

$$\begin{aligned}\hat{\mathcal{E}}_c^{(+)}(t) &= \int g(k)\hat{c}_k(t) \\ &= \int g(k)\hat{c}_k(0)e^{-i(k-\Delta_2)t} \\ &\quad -i\left[\frac{\gamma_c}{\pi}\right]^{1/2}\Gamma\int_0^t e^{-i(k-\Delta_2)(t-t')}\hat{\sigma}(t')dt' \ . \end{aligned} \tag{A1}$$

Employing

$$g(k)=\left[\frac{\gamma_c}{\pi}\right]^{1/2}\left[\frac{\Gamma}{\Gamma-ik}\right] , \tag{A2}$$

we observe that $\hat{\mathcal{E}}_c^{(+)}$ fulfills

$$\frac{d\hat{\mathcal{E}}_c^{(+)}(t)}{dt}=-(\Gamma-i\Delta_2)\hat{\mathcal{E}}_c^{(+)}(t)+\hat{F}^{(+)}(t)-i\gamma_c\Gamma\hat{\sigma}(t) , \tag{A3}$$

where $\hat{F}^{(+)}(t)$ is a quantum white noise. Denoting the vector

$$\boldsymbol{\alpha}_{nm}=\begin{bmatrix}\alpha_{nm}^1\\ \alpha_{nm}^2\\ \alpha_{nm}^3\end{bmatrix} =\begin{bmatrix}\langle(\hat{\mathcal{E}}_c^{(-)})^n\hat{\sigma}(\hat{\mathcal{E}}_c^{(+)})^m\rangle\\ \langle(\hat{\mathcal{E}}_c^{(-)})^n\hat{\sigma}^\dagger(\hat{\mathcal{E}}_c^{(+)})^m\rangle\\ \langle(\hat{\mathcal{E}}_c^{(-)})^n\hat{\sigma}_3(\hat{\mathcal{E}}_c^{(+)})^m\rangle\end{bmatrix} \tag{A4}$$

and

$$\beta_{nm}=[\langle(\hat{\mathcal{E}}_c^{(-)})^n(\hat{\mathcal{E}}_c^{(+)})^m\rangle] , \tag{A5}$$

we may use Eq. (A3) together with the Heisenberg equations for the atomic operators to derive a hierarchy of equations for the α's and β's.

In the Laplace-transformed form, they are

$$\begin{aligned}[z+G+(n+m)\Gamma+i(n-m)\Delta_2]\boldsymbol{\alpha}_{nm} &= \frac{i\gamma_c\Gamma}{2}(Mn\boldsymbol{\alpha}_{n-1m}-M^*m\boldsymbol{\alpha}_{nm-1}) \\ &\quad +\frac{i\gamma_c\Gamma}{2}(n\mathbf{e}_1\beta_{n-1m}-m\mathbf{e}_2\beta_{nm-1}) \\ &\quad +iM\boldsymbol{\alpha}_{nm+1}-iM^*\boldsymbol{\alpha}_{n+1m}-2\gamma_b\mathbf{e}_3\beta_{nm} , \end{aligned} \tag{A6a}$$

$$[z+(n+m)\Gamma+i(n-m)\Delta_2]\beta_{nm}$$
$$=i\gamma_c\Gamma(n\alpha^2_{n-1m}-m\alpha^1_{nm-1}) , \quad \text{(A6b)}$$

where

$$e_1=\begin{bmatrix}1\\0\\0\end{bmatrix},\ e_2=\begin{bmatrix}0\\1\\0\end{bmatrix},\ e_3=\begin{bmatrix}0\\0\\1\end{bmatrix}, \quad \text{(A7)}$$

while the matrices

$$M=\begin{bmatrix}0&0&1\\0&0&0\\0&-2&0\end{bmatrix},\ M^*=\begin{bmatrix}0&0&0\\0&0&1\\-2&0&0\end{bmatrix}, \quad \text{(A8)}$$

and

$$G=\begin{bmatrix}\gamma_b-i\Delta_1&0&-i\Omega/2\\0&\gamma_b+i\Delta_1&i\Omega/2\\-i\Omega&+i\Omega&2\gamma_b\end{bmatrix}. \quad \text{(A9)}$$

In order to solve Eqs. (A6), one has to break the infinite hierarchy. We used the method which simply decouples the equations for α_{nm} from α_{n+1m} (α_{nm+1}) employing

$$\alpha^1_{n+1m}=-i\gamma_c\Gamma\int_0^t e^{-(\Gamma-i\Delta_2)(t-t')}$$
$$\times\langle[\hat{\mathcal{E}}_c^{(-)}(t)]^n\hat{\sigma}(t')\hat{\sigma}(t)[\hat{\mathcal{E}}_c(t)]^m\rangle , \quad \text{(A10)}$$

etc., and calculating the right-hand side of Eq. (A10) up to the lowest order in γ_c/Γ. This method is a natural generalization of the one we have used to obtain our modified Bloch equations (24).

---

*Permanent address: Institute for Theoretical Physics, Polish Academy of Sciences, 02-668 Warsaw, Poland.

[1]E. M. Purcell, Phys. Rev. **69**, 681 (1946).
[2]D. Kleppner, Phys. Rev. Lett. **47**, 233 (1981).
[3]P. Goy, J. M. Raimond, M. Gross, and S. Haroche, Phys. Rev. Lett. **50**, 1903 (1983); R. G. Hulet, E. S. Hilfer, and D. Kleppner, *ibid.* **55**, 2137 (1985); W. Jhe, A. Anderson, E. A. Hinds, D. Meschede, L. Moi, and S. Haroche, *ibid.* **58**, 666 (1987).
[4]D. J. Heinzen, J. J. Childs, J. E. Thomas, and M. S. Feld, Phys. Rev. Lett. **58**, 1320 (1987).
[5]M. Lewenstein, T. W. Mossberg, and R. J. Glauber, Phys. Rev. Lett. **59**, 775 (1987).
[6]L. A. Lugiato, in *Progress in Optics,* edited by E. Wolf (Elsevier, New York, 1984), Vol. 21; see also the special issue of the J. Opt. Soc. Am. B **2** (1) (1985).
[7]F. Casagrande and L. A. Lugiato, Nuovo Cimento B **55**, 173 (1980); P. D. Drummond and D. F. Walls, Phys. Rev. A **23**, 2563 (1981); L. A. Lugiato, F. Casagrande, and L. Pizzuto, *ibid.* **26**, 3438 (1982).
[8]H. J. Carmichael and D. F. Walls, J. Phys. B **9**, 1199 (1976).
[9]D. F. Walls, Nature **306**, 141 (1983), and references therein; Squeezing effects in optical bistability were predicted by L. A. Lugiato and G. Strini, Opt. Commun. **41**, 67 (1982).
[10]D. F. Walls and P. Zoller, Phys. Rev. Lett. **47**, 709 (1981).
[11]H. J. Carmichael, Phys. Rev. Lett. **55**, 2790 (1985).
[12]L. A. Lugiato, Phys. Rev. A **33**, 4079 (1986).
[13]J. J. Sanchez-Mondragon, N. B. Narozhny, and J. H. Eberly, Phys. Rev. Lett. **51**, 550 (1983); G. S. Agarwal, *ibid.* **53**, 1732 (1984).
[14]E. T. Jaynes and F. W. Cummings, Proc. IEEE **51**, 89 (1963).
[15]M. G. Raizen, L. A. Orozco, M. Xiao, T. L. Boyd, and H. J. Kimble, Phys. Rev. Lett. **59**, 198 (1987).
[16]M. Lewenstein and T. W. Mossberg (unpublished).
[17]S. Haroche and J. M. Raimond, Adv. At. Mol. Phys. **20**, 350 (1985); J. A. C. Gallas, G. Leuchs, H. Walther, and H. Figger, *ibid.* **20**, 414 (1985).
[18]F. W. Cummings, Phys. Rev. **140**, A1051 (1965).
[19]J. H. Eberly, N. B. Narozhny, and J. J. Sanchez-Mondragon, Phys. Rev. Lett. **44**, 1323 (1980).
[20]G. Rempe, H. Walther, and N. Klein, Phys. Rev. Lett. **58**, 353 (1987).
[21]P. Filipowicz, J. Javanainen, and P. Meystre, Opt. Commun. **58**, 327 (1986); D. Meschede, H. Walther, and G. Muller, Phys. Rev. Lett. **54**, 551 (1985).
[22]B. R. Mollow, Phys. Rev. **188**, 1969 (1969).
[23]L. Allen and J. H. Eberly, *Optical Resonance and Two-Level Atoms* (Wiley, New York, 1975).
[24]C. P. Slichter, *Principles of Magnetic Resonance* (Springer-Verlag, Berlin, 1980).
[25]Y. S. Bai, A. G. Yodh, and T. W. Mossberg, Phys. Rev. Lett. **55**, 1277 (1985); N. Lu, P. R. Berman, A. G. Yodh, Y. S. Bai, and T. W. Mossberg, Phys. Rev. A **33**, 3956 (1986).
[26]E. Courtens and A. Szoke, Phys. Rev. A **15**, 1588 (1977); D. Grischkowsky, *ibid.* **14**, 802 (1976).
[27]W. H. Louisell, *Quantum Statistical Properties of Radiation* (Wiley, New York, 1973); G. S. Argarwal, in *Quantum Statistical Theories of Spontaneous Emission and their Relation to other Approaches,* Vol. 70 of *Springer Tracts of Modern Physics,* edited by G. Hohler and E. Niekisch (Springer-Verlag, Berlin, 1974), p. 1.
[28]P. R. Berman, J. Opt. Soc. Am. B **3**, 564 (1986); K. Wodkiewicz and J. H. Eberly, Phys. Rev. A **32**, 992 (1985); A. Schenzle, M. Mitsunaga, R. G. DeVoe, and R. G. Brewer, *ibid.* **30**, 325 (1984); G. S. Agarwal, Opt. Acta **32**, 981 (1985); A. G. Yodh, J. E. Golub, N. W. Carlson, and T. W. Mossberg, Phys. Rev. Lett. **53**, 659 (1984).
[29]G. S. Agarwal, R. K. Bullough, and G. P. Hildred, Opt. Commun. **59**, 23 (1986).
[30]See, for example, P. Zoller, G. Alber, and R. Salvador, Phys. Rev. A **24**, 398 (1981); A. T. Georges and S. N. Dixit, *ibid.* **23**, 2580 (1981); K. Wodkiewicz, Z. Phys. B **42**, 95 (1981).
[31]Z. Deng and S. Mukamel, Phys. Rev. A **29**, 1914 (1983).
[32]K. Rzazewski and J. H. Eberly, Phys. Rev. Lett. **47**, 408 (1981); for a review, see K. Rzazewski, in *Quantum Electrodynamics and Quantum Optics,* edited by A. O. Barut (Ple-

num, New York, 1984), p. 237.

[33]K. Rzazewski and J. Mostowski, Phys. Rev. A **35**, 4414 (1987); R. J. Kuklinski and K. Rzazewski (unpublished).

[34]A Lorentzian approximates the cavity density of modes in the vicinity of a particular cavity resonance. In general, the density of modes should be described by a formula analogous to the Airy formula for Fabry-Perot interferometers. See M. Born and E. Wolf, *Principles of Optics* (Pergamon, Oxford, 1975), p. 329.

[35]J. H. Eberly and K. Wodkiewicz, J. Opt. Soc. Am. **67**, 1252 (1977).

[36]C. Cohen-Tannoudji and S. Reynaud, J. Phys. B. **10**, 365 (1977).

[37]K. Rzazewski, M. Lewenstein, and J. H. Eberly, J. Phys. B **15**, L661 (1982); J. Zakrzewski, K. Rzazewski, and M. Lewenstein, *ibid*. **17**, 728 (1984).

[38]M. J. Collet and D. F. Walls, Phys. Rev. A **32**, 2887 (1985).